


Cite this: *Chem. Sci.*, 2017, 8, 6092

# Synthesis of 'reactive' and covalent polymeric multilayer coatings with durable superoleophobic and superoleophilic properties under water†

Dibyangana Parbat and Uttam Manna \*

Bioinspired underwater super-oil-wettability (superoleophilic/superoleophobic) properties are emerging as a potential avenue for developing smart materials for addressing issues related to healthcare, environment, energy, etc. However, the inherent poor durability of the materials that are mostly developed using polymeric hydrogel, metal oxide coatings and electrostatic multilayers often challenges the application of these wettability properties in practical scenarios. Here, 'amine-reactive' polymeric multilayers of nano-complex were developed to fabricate 'internal' underwater superoleophobic/superoleophilic coatings with impeccable physical/chemical durability. This allows the super-wetting properties to exist beyond the surface of the material and remain intact even after severe physical damage including erosion of the material and continuous exposure to an artificial-marine environment for more than 80 days. Moreover, this current design allowed for independent revalidation of some key hypotheses with direct experimental demonstrations, and provided a basis to develop highly durable super-oil-wettability properties under water. It is believed that this contemporary study will make a worthwhile contribution on developing multifunctional materials for widespread practical applications by exploiting these super-oil-wetting properties.

Received 8th March 2017

Accepted 6th June 2017

DOI: 10.1039/c7sc01055a

rsc.li/chemical-science

## Introduction

Under-water superoleophobic materials—those possessing both superoleophilic and superhydrophilic properties in air—can strongly repel liquid-oil droplets (with an advancing oil CA >150° and contact angle hysteresis <5°) under water.<sup>1–3</sup> Synthesis of such underwater superoleophobic coatings, which were inspired by fish scale features,<sup>4</sup> is of potential interest in various basic and applied contexts including anti-bio-fouling coatings, rapid oil/water separation, marine anti-fouling coatings, synthesis of efficient organic field-effect transistors, etc.<sup>2,6–11</sup> The general requirements for developing such coatings are quite unusual in comparison to the conventional fluorine-based superoleophobic property that displays extreme oil-

repellency mostly in air.<sup>12,13</sup> The underwater anti-oil-wetting property is often explained using the Cassie–Baxter model, where the trapped liquid water layer within the material contributes to the heterogeneous wetting of liquid-oil on the coated substrate under water.<sup>4,5</sup> So, the fabrication of a hierarchical surface topography composed of high surface energy materials is hypothesized to adopt desired underwater superhydrophobic properties. Jiang and co-workers first introduced an artificial underwater superoleophobic coating by mimicking the topography of fish scales using polyacrylamide (PAM) hydrogel.<sup>4</sup> Thereafter, various materials were developed to obtain such underwater superoleophobic properties,<sup>4,9,10,14–19</sup> mostly based on polymeric hydrogel<sup>4,9,10,18–20</sup> and metal oxide<sup>14,21–23</sup> coatings, which are highly susceptible to erosion in harsh physical/chemical environments (such as extremes of pH, salt, etc.).<sup>24</sup> However, such approaches are well recognized and widely practiced in the literature as they are known to reveal both the fundamentals and prospective applications of this anti-wetting property. Examples of durable coatings that can withstand severe chemical/physical treatments are still rare in the literature,<sup>10,24</sup> and further development is essential to synthesize highly robust underwater superoleophobic coatings.

In the recent past, the pursuance of oil/water separation has emerged as an important research theme due to the growing risk of water pollution from frequent oil spill accidents and the continuous discharge of industrial (oil-contaminated) wastewater.<sup>2,11</sup> The underwater anti-oil-fouling property is recognised

Department of Chemistry, Indian Institute of Technology-Guwahati, Kamrup, Assam 781039, India. E-mail: umanna@iitg.ernet.in

† Electronic supplementary information (ESI) available: Fig. S1–S15 accounting the growth of NC with and without the LbL deposition process, detailed comparisons of the multilayers of BPEI and NC, the change in the underwater oil-wettability with increasing deposition cycles of NC, the change in the optical transparency of the multilayers under water, the underwater oil-wettability of various model oils on post-modified multilayers of NC, bouncing of oil droplets underwater, the change in adhesive interactions with LbL deposition of NC, beading and wetting of oil droplets on post-modified multilayers under water, the effect of heating, freezing, and chemical and physical insults on the oil-wettability of the multilayers under water, LbL coating of various substrates, the guided transfer of oil droplets under water and the cleaning of oil using superoleophilic cotton under water. See DOI: 10.1039/c7sc01055a



for its self-cleaning ability, which together with the anti-fouling property provides a highly efficient avenue to separate/collect water from aqueous-oil contamination (emulsified or non-emulsified).<sup>7,16,19–21</sup> Another underwater super-wetting property known as underwater superoleophilicity,<sup>25,26</sup> which completely soaks up oils (with a contact angle of 0°)<sup>25</sup> under water, recently appeared in efficient materials that both separate and collect oil from aqueous media<sup>25–27</sup> and clean oil-contaminated surfaces. It was recently observed that such oil-wetting properties<sup>25–29</sup> often (with rare exceptions<sup>25,30</sup>) collapse in the absence of particular stimuli.<sup>26–29</sup> Examples of these various stimuli-responsive underwater superoleophilic materials are useful in specific proof-of-concept demonstrations, but a material with durable super-oil-wetting properties may further enlighten the path to several prospective and convenient applications in various practical settings including extremes of pH, salt, and other complex chemical scenarios.

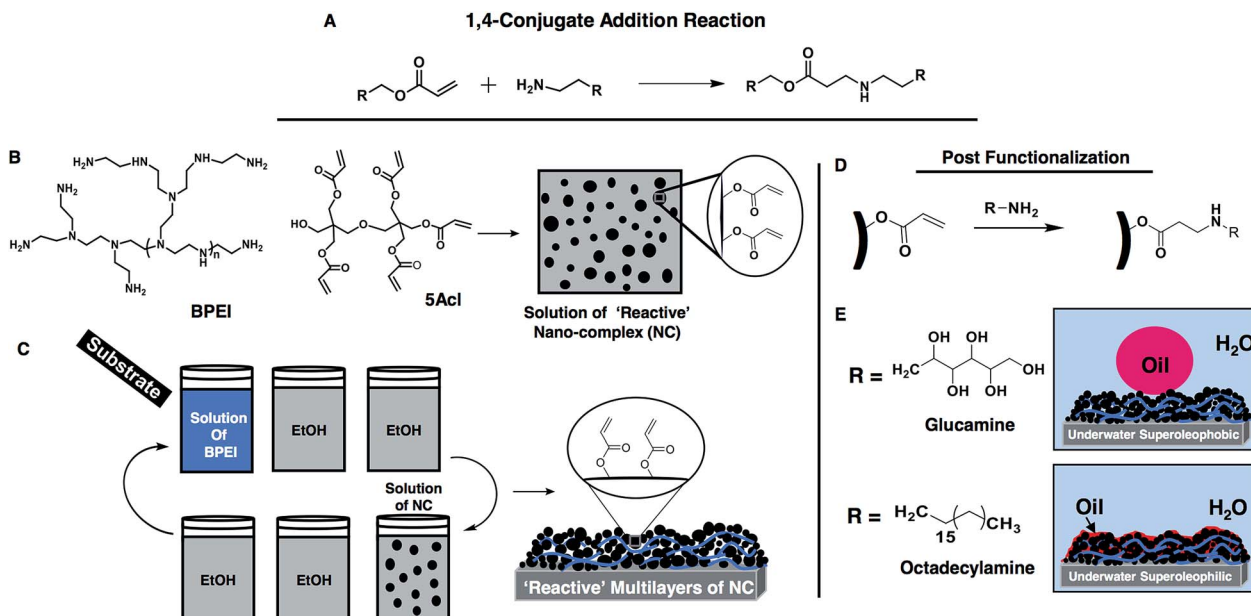
The work presented here is primarily motivated from past demonstrations, where several functional materials are fabricated by exploiting the robust Michael addition reaction<sup>31–35</sup> between primary amines and acrylates at ambient conditions including (1) synthesis of polymer coatings with various complex nanostructures,<sup>33,35</sup> (2) dendritic amplification of desired functional groups,<sup>34</sup> and (3) selective and three-dimensional (3D) functionalization of polymer microstructures.<sup>31</sup> This facile chemical approach is found to be appropriate for tailoring both the chemistry and the topography of the material.<sup>31–35</sup> Here, we introduce an amine-‘reactive’ multilayer of a polymeric nano-complex (NC) exploiting the 1,4-conjugate addition reaction between the amine and acrylate groups of

branched poly(ethyleneimine) (BPEI, polymer) and dipentaerythritol penta-/hexa-acrylate (5Acl, small molecule), respectively (Scheme 1A and B), to synthesize (1) covalently cross-linked, (2) thicker, (3) chemically/physically durable, (4) optically transparent, and (5) substrate-independent polymeric coatings with ‘internal’ (including both surface and interior) underwater superoleophobic/superoleophilic properties, which is unprecedented in the literature. This current design has been further explored to reveal the fundamentals of the extremes of oil-wettability under water in detail. In the recent past, Wang and coworkers<sup>29</sup> hypothesized the role of a trapped air layer in achieving continuous and discontinuous three-phase contact lines (TPCLs), which eventually controlled the underwater wettability of oil droplets at the multi-phase interfaces. Here, in our present design, we have developed continuous (for superoleophobicity) and discontinuous (for superoleophilicity) TPCLs just by adopting the appropriate chemistry in the material through strategic and facile post-chemical modification of the ‘reactive’ multilayers of NC, to control the underwater oil-wettability on solid surfaces as shown in Scheme 1C.

## Results

### Synthesis of reactive and covalent multilayers and characterizations

Recently, we reported<sup>36</sup> the fabrication of an amine-‘reactive’ polymeric gel from a mixture (with an appropriate composition) of BPEI/5Acl in ethanol under ambient conditions, where the polymer (BPEI) and the multifunctional small molecule (5Acl) readily reacted through the Michael addition reaction and



**Scheme 1** (A) The 1,4-conjugate addition reaction between primary amine and acrylate groups. (B) The chemical structures of poly(ethyleneimine) (BPEI) and dipentaerythritol penta-acrylate (5Acl). Mixing of these chemicals in ethanol provides amine-‘reactive’ nano-complexes. (C) A schematic illustrating the construction of the ‘reactive’ multilayer by covalent LbL deposition of the ‘reactive’ nano-complex and BPEI. (D and E) Post-chemical modification of the multilayers with primary amine-containing small molecules (glucamine and octadecylamine) providing underwater superoleophobicity/superoleophilicity.



formed a nano-complex that eventually aggregated into a polymeric gel material and was allowed to develop into a self-standing superhydrophobic material. Here, we have exploited the same facile chemistry in developing a thick and porous polymeric multilayer (that is reactive) for achieving both superoleophilicity and superoleophobicity under water. First, we selected a composition of BPEI/5Acl in ethanol that provided a stable dispersion of the growing nano-complex solution (Fig. 1A: black curve and Fig. S1H–M†). The formation of the nano-complex and its growth were investigated by visual inspection and a dynamic light scattering (DLS) study, where a faint turbid mixture of the NC (size  $\sim 98$  nm) solution became a highly opaque and milky solution (size  $\sim 198$  nm) within  $\sim 3$  min, and the size of the nano-complex was observed to grow further with time without any sedimentation even after  $\sim 21$  min (size  $\sim 522$  nm) (Fig. 1A: grey curve and Fig. S1C–G†). The same reaction mixture of BPEI/5Acl, which was not used in successive LbL depositions, was also capable of forming NC, however the growth of the NC was slow. The accelerated growth of the NC in the BPEI/5Acl mixture during LbL depositions is likely due to the gradual and the additional transfer of branched polymer from the BPEI solution to the BPEI/5Acl mixture through consecutive dipping of the substrates in these dipping solutions (Scheme 1C). Then, this dispersion of the nano-complexes was thoroughly washed with ethanol prior to

examination by FTIR spectroscopy. Two characteristic signatures at  $1739\text{ cm}^{-1}$  and  $1409\text{ cm}^{-1}$ , which represented the carbonyl stretch and the symmetric deformation of the C–H bond for the  $\beta$  carbon of the vinyl groups, respectively, revealed the presence of residual acrylate groups in the polymeric nano-complexes. Furthermore, the depletion of the characteristic peak intensity at  $1409\text{ cm}^{-1}$  for the residual acrylate moieties upon treatment with primary amine-containing small molecules unambiguously suggested the existence of exceptional chemical reactivity (Fig. S1N;† propylamine).

These chemically active residual acrylate groups in the polymeric NC provided a basis to develop a covalently cross-linked multilayer of the polymeric NC in combination with the amine-containing BPEI polymer through consecutive 1,4-Michael addition reactions (Scheme 1A). During the LbL deposition process, a similar polymeric NC solution was noticed to grow faster (black curve, Fig. 1A), without having any noticeable sedimentation of NC. The layer-by-layer growth of this NC multilayer was monitored by measuring the thickness of the assembly, which grew exponentially with deposition cycles (the deposition of BPEI and NC at each LbL-cycle is labelled as one bilayer) and the thickness of the NC multilayer (20 bilayers) was measured to be  $2.2\text{ }\mu\text{m}$  (Fig. 1B, black curve). In comparison, the LbL growth of the BPEI/5Acl multilayer, which was constructed from separate solutions of BPEI and 5Acl, was

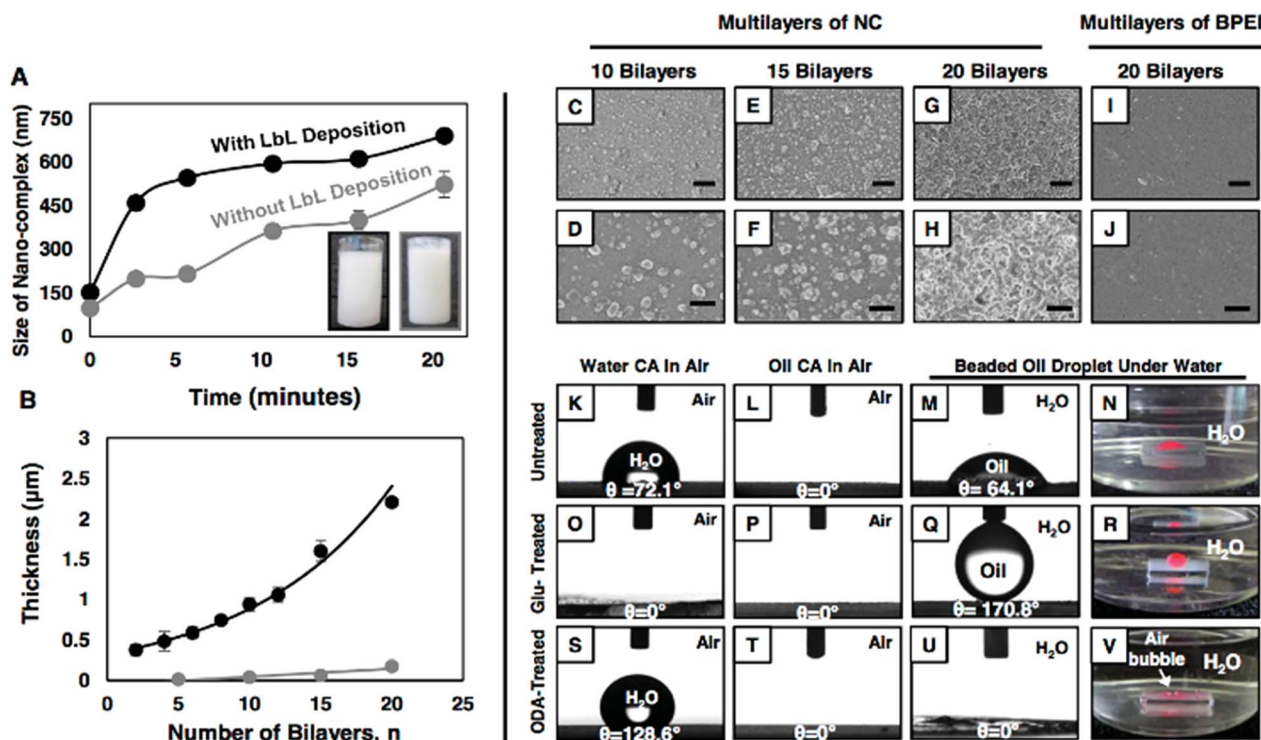


Fig. 1 (A) The growth of nano-complexes with time during LbL deposition (black) and without LbL deposition (grey), inset showing digital images of those milky turbid solutions after 21 min. (B) The growth (thickness vs. number of bilayers) of LbL coatings that are composed of NC/BPEI (black) and BPEI/5Acl (grey). (C–H) FESEM images of the ‘reactive’ multilayers of NC showing the changes in the morphology of the coatings with increasing bilayer depositions (10 (C and D), 15 (E and F) and 20 (G and H) bilayers) in low (C, E, and G; scale-bar:  $10\text{ }\mu\text{m}$ ) and high (D, F, and H; scale-bar:  $3\text{ }\mu\text{m}$ ) magnifications. (I and J) FESEM images of multilayers (20 bilayers) of BPEI/5Acl in low (I; scale-bar:  $10\text{ }\mu\text{m}$ ) and high (J; scale-bar:  $3\text{ }\mu\text{m}$ ) magnifications. Contact angle images (K–M, O–Q, S–U) and digital images (N, R, V) illustrating the wetting of water in air (K, O, S) and oil both in air (L, P, T) and under water (M, N, Q, R, U and V).



observed to be significantly sluggish (the thickness of the multilayer was only 174.09 nm, even after 20 cycles of LbL-depositions) and linear (Fig. 1B, grey curve) as the branched polymer (BPEI) was only deposited through mutual covalent reactions with small molecules (5Acl), whereas, in the previous multilayer's construction, both the NC and the BPEI polymer were consecutively deposited, and yielded a much thicker coating. Furthermore, the change in the topography of the multilayers of NC as the bilayer deposition increased was monitored with FESEM imaging (Fig. 1C–H). An arbitrary hierarchical and porous topography was observed in the 20-bilayered NC multilayer (Fig. 1G and H), whereas the topography of the multilayers (20 bilayers) of BPEI/5Acl was noticed to be featureless and smooth (Fig. 1I and J). The regular change in the morphology in the multilayer assembly was exploited later in revealing the role of surface topography behind the underwater oil-wettability property.

### Characterization of super-oil-wettability under water

Furthermore, the appearance of two characteristic peaks at  $1739\text{ cm}^{-1}$  and  $1409\text{ cm}^{-1}$  (for carbonyl stretch and symmetric deformation of the C–H bond for the  $\beta$  carbon of the vinyl groups, respectively) in the FTIR spectrum of the multilayers (20 bilayers) of NC revealed the existence of residual acrylate moieties in the NC-assembly, even after successive covalent LbL deposition (Fig. S2I† red curve). Then, both oil and water wettability were examined on the 'reactive' NC multilayer (20 bilayers) both in air and under water. The hydrophilic (with a water CA of  $72.1^\circ$ ) and superoleophilic (with an oil CA of  $0^\circ$ ) NC multilayers in air were found to be inherently oleophilic under water with an oil CA  $\sim 64.1^\circ$  (Fig. 1K–M), likely due to the preferable interaction of the beaded oil droplet with the hydrophobic residual acrylate groups present in the NC multilayer. However, the post chemical modification of the NC multilayer with strategically selected small molecules (hydrophilic: glucamine and hydrophobic: octadecylamine) through a 1,4-conjugate addition reaction provided both superoleophobic (an advancing OCA of  $170.8^\circ$ ; Fig. 1O–R) and superoleophilic (an OCA of  $0^\circ$ , Fig. 1S–V) properties to the material under water. The successful covalent modifications on the NC multilayer with amine-containing small molecules (glucamine and octadecylamine) were characterized further with detailed FTIR analysis (Fig. S2I†). In comparison, after post-chemical modification with glucamine, the featureless (Fig. S2G†) and underwater oleophilic (OCA of  $25.5^\circ$ ) multilayer of BPEI/5Acl displayed underwater oleophobicity with an OCA of  $123.8^\circ$ , however, the post-modification of the same multilayer with octadecylamine had a minute effect on the underwater oil-wettability (Fig. S2A–C†). Thus, this study further revealed the need for a porous hierarchical topography to achieve underwater superoleophobicity. Moreover, it was noticed that the underwater oil-wettability of both the Glu- and ODA-modified NC multilayers was varied by increasing the number of bilayer depositions: the underwater static-OCA gradually increased from  $135.6^\circ$  (2 bilayers) to  $165.2^\circ$  (20 bilayers) for the glucamine-treated NC multilayer (Fig. S3A–E†) with little compromise in

the underwater optical transparency (Fig. S4†), whereas the ODA-treatment transformed oleophilicity ( $29.9^\circ$ ) into superoleophilicity ( $0^\circ$ ) in the material by increasing the LbL deposition (Fig. S3F–J†). Thus, this current study confirmed the need for appropriate chemical (hydrophilic/hydrophobic) and physical (surface topography) parameters to achieve the desired underwater super-wettability. Moreover, both of these Glu- and ODA-treated NC multilayers were capable of displaying extremes of wetting phenomena with a wide range (with respect to surface tension) of water immiscible model oils from hexane ( $17.89\text{ mN m}^{-1}$ ) to DCE ( $32.2\text{ mN m}^{-1}$ ) (Fig. S5†).

On dropping a model-oil (DCM) droplet ( $11\ \mu\text{L}$ ) on to the Glu-treated NC multilayer (20 bilayers) from a distance of 12.5 mm, it was noted that the oil droplet bounced before eventually settling on the multilayer with an OCA of  $\sim 165^\circ$  (Fig. 2A–E). The beaded oil droplet readily rolled off (Fig. S6†) when the surface was tilted at  $3^\circ$ . This extreme oil-repellency under water is often explained using the Cassie–Baxter model,<sup>4</sup> where the heterogeneous wetting of oil on an NC multilayer is due to impregnation and confinement of liquid water within the hierarchically featured surface. The confined water layer within the Glu-treated porous NC multilayer depreciated the contact area of the beaded oil droplet with the NC multilayer (Fig. 2K). Furthermore, the fraction of the fluid (oil, beaded DCM droplet) area in contact with the Glu-treated NC multilayer was estimated using eqn (1) and eqn (2), where  $\theta$  and  $\theta_r$  are the oil-contact angles on the multilayers (20 bilayers) of BPEI/5Acl (smooth surface, glucamine- $123.8^\circ$ ) and NC (porous, glucamine- $165.2^\circ$ ), respectively.

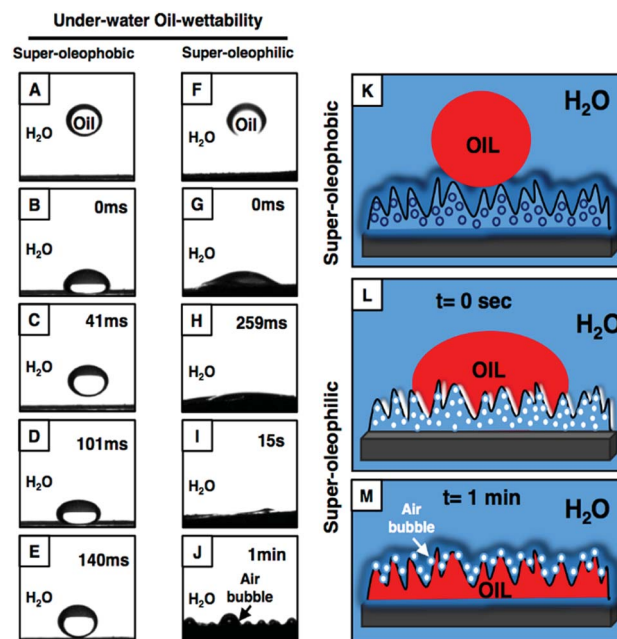


Fig. 2 (A–J) Contact angle images showing the bouncing (A–E) and spreading (F–J) of oil droplets ( $11\ \mu\text{L}$  of DCM) on the glucamine- and ODA-treated NC multilayers, respectively, under water. (K–M) A schematic illustration of underwater beading/wetting of oil droplets on superoleophobic (K)/superoleophilic (L and M) materials.



$$\cos \theta_r = f_1 \cos \theta - f_2 \quad (1)$$

$$f_1 + f_2 = 1 \quad (2)$$

The fractions of the solid contact area and the trapped water (in NC multilayers) contact area with the beaded oil droplet are labelled as  $f_1$  and  $f_2$ , respectively. The estimated fraction of the contact area of the beaded oil droplet on the Glu-treated NC multilayer (20 bilayers) was 0.075, whereas the values were 0.621 and 0.86 for the 15- and 10-bilayer multilayers (Glu-treated), respectively, and the higher contact area between the beaded oil droplet and the NC multilayers induced more adhesive interaction between them (Fig. S7†). This is mostly because of the difference in the surface topography of the multilayers as confirmed by the FESEM study (Fig. 1C–F). The topography of the solid interfaces plays a critical role in controlling the adhesive interaction of the beaded liquid droplet on the solid interfaces,<sup>37</sup> and the appropriate hierarchical topography is essential to lower (Cassie state) the contact area between the beaded oil droplet and the solid interfaces. Here, the NC multilayer was inherently decorated with an essential hierarchical topography after 20 bilayers of NC depositions (1G and H), and eventually displayed non-adhesive superoleophobicity under water. However, the less prominent microdomains in the NC multilayer after 10 (1C and D) and 15 (1E and F) bilayers of NC depositions were attributed to the higher contact area between the beaded oil droplet and the NC multilayer, and eventually the multilayer adopted a Cassie–Wenzel transition state.<sup>37</sup> However, dropping the oil droplet on the ODA-treated NC multilayer led to spontaneous wetting and spreading of the oil droplet with an OCA of 0° (Fig. 2F–J, L and M). Immediately, the trapped air in the multilayer (2.2 μm) was released to the surface of the material, which was observed with the naked eye (Fig. 2J and M). This demonstration revalidated the existence of hypothesized trapped air that provides a discontinuous TPCL in the multilayer.

### Physical/chemical durability of underwater super-oil-wettability properties

Next, this covalently cross-linked NC multilayer was exposed to various complex and harsh physical/chemical settings to investigate the durability of the underwater extreme-wetting properties of the material.

First, this Glu-treated NC multilayer was treated with water steam, however no apparent change in the anti-wetting property was noticed (Fig. 3A and D) after the treatment. Additionally, the Glu-treated multilayer was exposed to elevated temperature, and on increasing the temperature of the water phase, the size of the beaded oil droplet (Fig. 3B and G,  $\theta_{Adv.} \sim 171^\circ$ ) on the multilayer-coated substrate was observed to shrink (Fig. 3G–I) as the oil-phase gradually evaporated out at the elevated temperature. The droplet eventually disappeared at 100 °C (Fig. 3J), however, the underwater superoleophobic property of the material remained intact during (Fig. S10A–P,†  $\theta_{Adv.} \sim 170^\circ$ ) and after this process (Fig. 3E).

An underwater beaded oil droplet (Fig. 3C,  $\theta_{Adv.} \sim 172^\circ$ ) was introduced on the Glu-treated multilayer at  $-20^\circ\text{C}$ . Over the time (2 h) the liquid water phase was frozen into ice (Fig. 3K), however, the shape of the beaded oil droplet remained intact before and after the freezing process (Fig. S10Q–S,†), which indicated that its underwater anti-fouling property remained unaltered during the whole process. The property remained unchanged after thawing the frozen ice with  $\theta_{Adv.} \sim 172^\circ$  (Fig. 3F). Then, the NC multilayer-coated glass substrates were separately submerged in DI-water and artificial seawater for continuous and prolonged (80 days) exposure, however, this material continued to display robust underwater anti-fouling properties with  $\theta_{Adv.} > 165^\circ$  and  $\theta_{hys.} \leq 5^\circ$  (Fig. 3L). Moreover, the underwater superoleophobic property remained intact with  $\theta_{Adv.} > 165^\circ$  (Fig. S11†), even after exposure of this Glu-treated NC multilayer to various harsh and complex aqueous systems including extremes of pH (pH 1 and pH 11) and surfactants (DTAB, SDS; 1 mM), and BSA protein (5%) contaminated aqueous phases. The impeccable chemical durability of the material and its anti-fouling property are mostly due to the existence of extensive covalent cross-linkages (through the 1,4-conjugate addition reaction) in the NC multilayer. Next, some standard physical abrasion tests including an adhesive tape test, a sand paper abrasion test, and a sand drop test were adopted to investigate the physical durability of the underwater super oil-wetting properties of the material. First sand paper (2 cm × 2 cm) was manually rubbed back and forth on the polymeric-material (1 cm × 1 cm) several times (five) with an applied load of 200 g, resulting in substantial erosion of the white powdery material (that adhered on the sand abrasion paper; Fig. S12G–H,†), however, both the Glu- and ODA-treated multilayers displayed super-wetting properties (Fig. 3M–P) without considerable changes in the OCA underwater, even after removal of the top surface of the coating. Thus, the current study revealed the existence of ‘internal’ underwater super-wettability properties in the NC multilayer. Such robust materials are rare in the literature. Furthermore, the FESEM image of the abraded multilayer revealed that the topography of the material (Fig. 3Q) was significantly different from the native coating (Fig. S12E and F,†), however, this physically damaged coating had appropriate hierarchical structures to display underwater super oil-wetting properties (Fig. S12I–L,†). The adhesive-tape test was performed on the multilayer, however, fracture or delamination of the material from the substrate was not noticed after the demonstration. Moreover, a very porous morphology with arbitrary arrangement of granular domains, which is similar to untreated material, was observed under FESEM study (Fig. 3V). As expected, the anti-wetting property remained unaffected even after the adhesive tape test (Fig. 3R–U). Lastly, the impact of sand grain (100 g) on the material from a distance of 20 cm was tested following standard protocol and the anti-wetting property was found to remain intact (Fig. S12M–P,†), without causing any noticeable physical damage to the material. Thus, the synthesized material displayed extraordinary tolerance to various physical insults including physical damage that eroded away the top surface of the material.



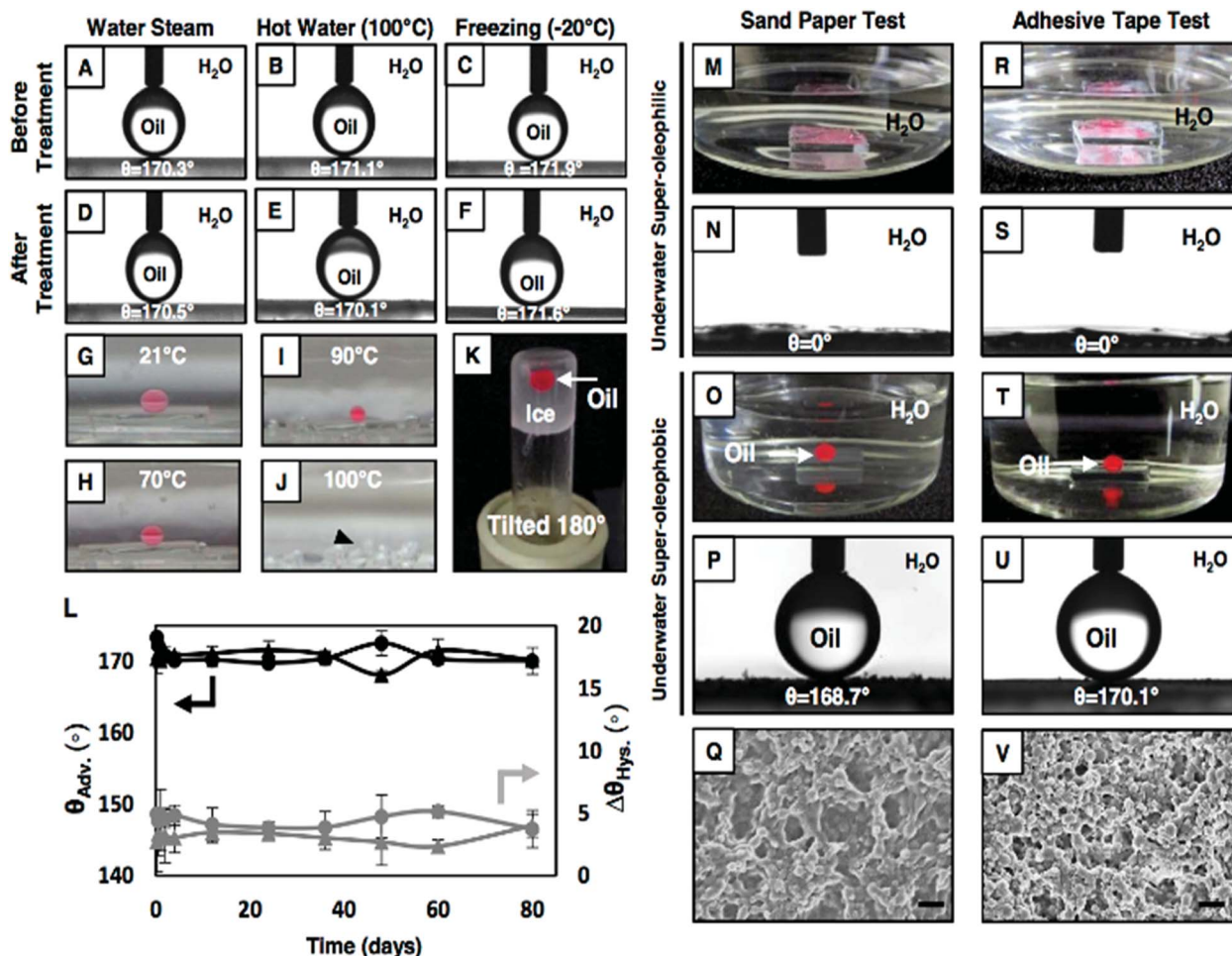


Fig. 3 Underwater advancing-OCA ( $\theta_{Adv.}$ ) on the glucamine-treated multilayers before (A–C) and after (D) water steam, (E) hot water (100 °C), and (F) freezing (–20 °C) treatments. (G–J) Digital images showing the change in the size of a beaded DCM droplet on a NC multilayer with increasing temperatures from 21 °C to 100 °C. (K) Digital image of a beaded oil droplet on a glucamine-treated NC multilayer after freezing the water phase at –20 °C, where the glass vial is tilted at 180°. (L) The plot showing the change in advancing-OCA (black) and contact angle hysteresis (grey) under deionized-water (circle) and artificial sea-water (triangle) for 80 days. (M–V) Digital images (M, O, R, and T) and contact angle images (N, P, S, and U) of the glucamine (O–P, T–U) and ODA-treated (M–N, R–S) multilayers after performing the sand-paper abrasion (M–P) and adhesive tape (R–U) tests. (Q, V) FESEM images (scale bar: 1  $\mu$ m) of the multilayer coating after the sand paper abrasion (Q) and adhesive tape (V) tests.

### Applications of super-oil-wettability properties in guided oil-transport and cleaning/preventing oil-contamination under water

The inherent ability of the LbL-deposition approach allowed various (rigid and flexible) objects to be coated with an NC multilayer, irrespective of the dimension and geometry of the substrates. The amine ‘reactive’ NC multilayers (20 bilayers) were deposited on underwater oleophilic (plastic film, OCA <30°: Fig. S13E†) and oleophobic (wood, sand paper and Al-foil, OCA >130°: Fig. S13A, I and M†) substrates, and strategic post-functionalization of these NC multilayers provided both underwater superoleophilic (Fig. S13C, G, K and O†) and superoleophobic properties (Fig. S13B, F, J and N†). A detailed account of the underwater OCA on both the bare and coated substrates is given in Table 1, where the ODA-treated multilayer instantly soaked up oil within the material and the glucamine-

treated multilayer strongly repelled oil with  $\theta_{Adv.} >165^\circ$  and  $\theta_{hys.} <10^\circ$ . Moreover, the interior of a glass tube (OCA  $\sim 124^\circ$ , Fig. 4A) could be successfully decorated with strong oil-repelling properties (OCA  $\sim 165^\circ$ , Fig. 4B), which was further used in demonstration of facile and guided transport of tiny (8  $\mu$ L) oil droplets under water, without any adhesion or loss of oil during the transportation process (Fig. 4D–F), which is impossible to achieve with a bare glass tube (Fig. 4C and S14G–L†). Thus, this proof-of-concept demonstration revealed the ability of this anti-wetting property in preventing unwanted oil-contaminations and in providing energy efficient and gravity driven guided transport of heavy oil or oily-material. The fibrous cotton, which has inherent underwater superoleophobicity (OCA  $\sim 169^\circ$ , Fig. 4H), was coated with this NC multilayer to achieve underwater superoleophilicity (Fig. 4G), and the material was further used in demonstrating (Fig. 4K and L) the cleaning of other oil-contaminated substrates (bare glass) (Fig. S15†).



Table 1 Accounts of the advancing-OCA and contact angle hysteresis on various uncoated and coated (Glu-/ODA-treated) substrates

Substrates	$\theta_{adv.}$ ( $^{\circ}$ )		$\theta_{hys.}$ ( $^{\circ}$ )		
	Uncoated	Glu-Treated	Uncoated	Glu-Treated	ODA Treated $\theta$ ( $^{\circ}$ )
Wood	136.2 $\pm$ 0.8	168.3 $\pm$ 0.7	15.8 $\pm$ 0.4	5.8 $\pm$ 0.8	0
Plastic	26.6 $\pm$ 0.4	167.2 $\pm$ 0.2	26.6 $\pm$ 0.4	6.4 $\pm$ 0.6	0
Sand paper	132.7 $\pm$ 0.3	167.8 $\pm$ 0.4	25.9 $\pm$ 0.5	2.0 $\pm$ 0.3	0
Al foil	137.9 $\pm$ 0.7	170.1 $\pm$ 0.5	20.9 $\pm$ 0.5	4.5 $\pm$ 0.6	0

## Discussion

Here, we have developed ‘amine-reactive’ covalently cross-linked multilayers of a nano-complex (NC) *via* a facile 1,4-conjugate addition reaction between the acrylate and primary amine groups of dipentaerythritol pentaacrylate (5Acl, multifunctional small molecules) and branched poly (ethyleneimine) (BPEI, polymer), respectively, in ethanol at ambient conditions. The consecutive layer-by-layer (LbL) deposition of the reactive (due to the presence of residual acrylate groups) and growing NC provided a basis to tailor both the topography and chemistry of the multilayers, and eventually allowed decoration of the material with essential fundamentals ((1) hierarchical topography and (2) appropriate chemistry), to achieve extremes of oil-wettability properties under water. This precise control over both the topography and chemistry of the multilayers further allowed the fundamentals behind the properties of underwater superoleophilicity and superoleophobicity to be revalidated independently with appropriate experimental demonstrations. The existence of meta-stable trapped air, which is hypothesized to be essential for underwater superoleophilicity, was experimentally revealed using our synthesized material. Furthermore, the controlled change in the morphology of the material (by strategic control of the LbL deposition cycles) in combination with appropriate post chemical modification of the ‘reactive’

multilayer provided a basis to tailor the underwater oil-wettability, starting from the superoleophilicity to the superoleophobicity. Moreover, the fraction of contact area between the beaded oil droplet and the glucamine-modified NC multilayers under water controlled the adhesive interaction, and eventually provided both the adhesive and non-adhesive superoleophobic coatings under water.

The covalently cross-linked and thick (2.2  $\mu\text{m}$ ) multilayer coatings that were strategically post-functionalized with amine-containing small molecules (glucamine and octadecylamine) yielded ‘internal’ superoleophilic and superoleophobic properties under water, where both the surface and interior of the multilayers were with the appropriate topography and chemistry to display robust super-oil-wetting properties under water. As a consequence, the underwater super-oil-wettability properties remained unperturbed even after severe physical damage, including removal of the top surface of the material, which destroyed both the surface topography and surface chemistry of the material. On the other hand, extensive covalent cross linkages through the 1,4-conjugate addition reaction between the acrylate and amine groups provided impeccable chemical stability to the material, and thus, the underwater superoleophilic and superoleophobic properties remained unaltered, even after continuous exposure to complex aqueous conditions including artificial sea water, extremes of pH and protein- and

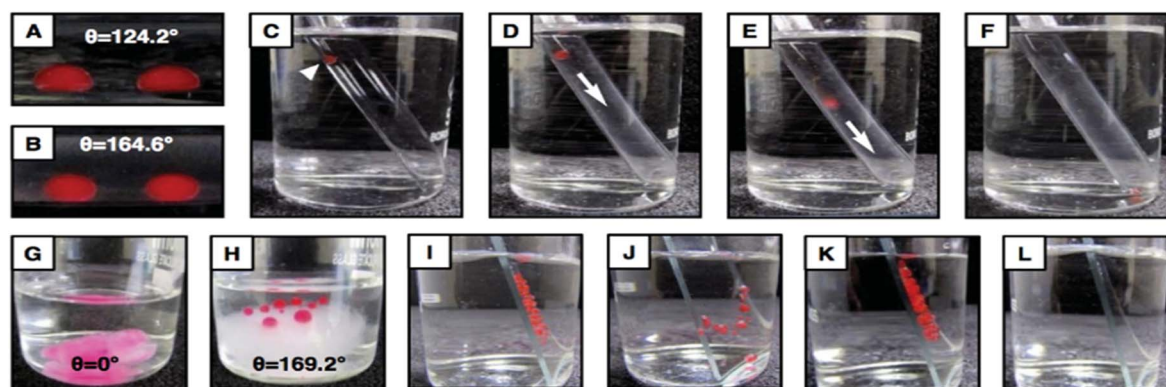
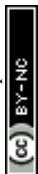


Fig. 4 (A and B) Digital images of underwater oil contact on both bare glass (A) and glucamine-modified multilayer coated glass (B). (C–F) Digital images illustrating the pinning (C) and rolling (D–F) of beaded oil droplets on both the bare (A) and multilayer (glucamine-treated; B) coated glass tube under water. (G and H) Beading and wetting of oil droplets on both bare cotton (H) and multilayer coated (ODA-treated, G) cotton under water. (I–L) Demonstration of the repulsive (I and J) and attractive (K and L) interactions of the immobilized oil droplets (on bare glass) with both the superoleophobic (H; bare cotton) and superoleophilic (G; ODA-treated-multilayer) cotton. The oil-contaminated surface was instantly cleaned by the multilayer-coated (ODA-treated, G) cotton, whereas bare cotton pushed/moved the immobilized oil droplets from one area to other.



surfactant-contaminated aqueous media. Furthermore, the anti-wetting property remained intact at raised temperatures (including boiling temperature), and during and after the freezing process. Thus, the current design provided underwater superoleophobic/superoleophilic coatings with exceptional physical and chemical durability.

This covalent and rapid LbL deposition process further allowed different types of substrates to be coated with durable super-oil-wetting properties under water including the surfaces of wood, plastic, metal *etc.* Moreover, the substrates with a complex geometry, including the interior of the glass tube and the fibrous cotton, could be decorated with desired oil-wetting properties under water. The glass tube that was coated with underwater superoleophobicity was further exploited in demonstrating the protection of the substrate from oil-contamination and guided oil-transport under water, whereas the cotton that was decorated with underwater superoleophilicity was found to be useful in the facile cleaning of oil-contaminated bare glass surfaces. Thus, both these super-oil-wetting properties provided complimentary approaches for self-cleaning (underwater superoleophobicity) and facile post-cleaning (underwater superoleophilicity) of oil-contaminations under water, which can also be seen as a leading approach to protect/prevent water pollution and for water purification.

## Conclusions

In conclusion, the design of amine-‘reactive’ NC multilayers provided insight about the fundamentals of underwater superoleophilic and superoleophobic properties in detail. The ‘reactive’ multilayers of NC provided a facile avenue to control both the chemistry and topography of the polymer coatings, and this fresh design independently revalidated some key hypotheses that explained the extremes of oil-wetting properties in detail. Moreover, the approach of using covalently cross-linked NC multilayers resulted in the desired ‘internal’ underwater super-oil-wettability properties, which can withstand various severe physical and chemical insults. Furthermore, the LbL deposition process allowed a wide range of substrates to be endowed with desired underwater super-wetting properties for both protecting the substrates from oil-contamination, and for cleaning oil from the oil-contaminated bare substrates. Current findings are anticipated to provide an avenue to further extend the horizon of bio-inspired underwater super oil-wetting properties for designing/developing advanced and multifunctional materials in the interest of a wide range of relevant applications in practical settings.

## Experimental

### Materials

Branched polyethyleneimine (BPEI, MW~ 25 000), tripentaerythritol penta-acrylate (5Acl, MW~ 524.21 g mol<sup>-1</sup>), propylamine, hexylamine, octylamine, decylamine, bovine serum albumin (BSA), sodium dodecyl sulphate (SDS), Nile red (Technical grade, Sigma-N3013) and dodecyltrimethylammonium bromide (DTAB) were purchased from

Sigma Aldrich, Bangalore, India. 1-Pentylamine, heptylamine, and 1-octadecylamine were obtained from Alfa-Aesar and *n*-butylamine and *n*-heptane were bought from Spectrochem Pvt. Ltd., Mumbai, India. HCl and dimethyl sulfoxide (DMSO) were purchased from Fischer Scientific, Mumbai, India. NaOH and toluene were bought from Merck Specialties Private, Ltd. Ethyl alcohol was purchased from TEDIA Company (United States of America). THF was obtained from RANKEM, Maharashtra, India. Sand paper (grit no. 400) was acquired from Million International, India. Microscopic glass slides were obtained from JSGW (Jain Scientific Glass Works, India) and aluminium foil (Parekh Aluminex Ltd., India) and adhesive tape (Jonson tape Ltd. India) were purchased from local sources. Dichloromethane (DCM), dichloroethane (DCE) and ethyl acetate were acquired from Merck Life Science Pvt. Ltd., New Delhi, India. D-glucamine (>95%) was purchased from TCI (Tokyo Chemical Industry). Hexane was purchased from Central Drug House Pvt. Ltd. (CDH), Mumbai, India. Sand and wood were obtained from a construction site at IIT-Guwahati, Assam.

### Characterization

The glass dipping vials were washed thoroughly with ethyl alcohol followed by acetone prior to preparing the LbL dipping solutions, and compressed air was used to dry the synthesized multilayers of the polymeric nano-complexes. Contact angles were measured at five different locations on each sample using the KRUSS Drop Shape Analyzer-DSA25 instrument with an automatic liquid dispenser at ambient temperature. A dynamic light scattering (DLS) study was performed using a Zetasizer Nano ZS90 instrument (model no. ZEN3690). All the samples were coated with a thin layer of gold using a gold sputterer prior to obtaining scanning electron microscopic images (SEM) of the multilayers using a Carl Zeiss field emission scanning electron microscope (FESEM). Fourier transform infrared spectra were recorded using a Perkin-Elmer FTIR spectrophotometer instrument at ambient temperature, where the polymeric matrix was mixed well with KBr prior to forming the KBr pallet. The digital images were captured using a Canon Power Shot SX420 IS digital camera. The optical transparency of the coating under water was measured using a Perkin-Elmer Lambda 750 (UV/VIS/NIR Spectrometer). The thickness of the coatings were estimated using a Veeco Dektak 150 surface profilometer.

### Preparation of the ‘reactive’ layer by layer (LBL) assembly

The solutions of 5Acl (265 mg ml<sup>-1</sup>) and BPEI (50 mg ml<sup>-1</sup>) in ethanol were prepared first in two separate glass vials. Then 500 μL of BPEI was mixed with 5Acl solution (5 ml) in ethanol and the mixture was kept with continuous agitation for 20 minutes to initiate the formation of the ‘reactive’ polymeric nano-complex (NC) (see text for more details). Then a clean glass slide (5.5 cm × 1 cm) was taken as a model substrate, where layer-by-layer (LbL) deposition of ‘reactive’ NC was achieved with the help of BPEI polymer solution in ethanol. The detailed LbL deposition process was as follows; (a) glass substrates were placed in a solution of BPEI for 10 seconds; (b) the substrates were removed and washed with an initial ethanol bath for 10





seconds followed by a second ethanol bath for another 10 seconds; (c) the substrates were placed in a stable dispersion of 'reactive' NC in ethanol for 10 seconds; and (d) substrates were removed from the 'reactive' NC solution and washed again, following the process described under step (b). This cycle was repeated 20 times to fabricate a porous polymeric multilayer consisting of 20 BPEI/NC layer pairs (each BPEI/NC layer pair is further denoted as 'bilayer' in the main text). Following similar protocol, we have developed another multilayer consisting of BPEI/5Acl, where 'reactive' NC solution was replaced with 5Acl solution (265 mg ml<sup>-1</sup> in ethanol). During the whole LbL deposition process, the concentrations of the polymer (or NC) solutions were maintained by the addition of ethanol as needed after regular intervals to compensate for solvent evaporation.

### Post-modification with desired amine-containing small molecules

The 'reactive' multilayers (20 bilayers) consisting of BPEI/NC were chemically post-functionalized with various amine-containing small molecules including propylamine (34.23 mg ml<sup>-1</sup>, in THF), butylamine (35.23 mg ml<sup>-1</sup>, in THF), pentylamine (35.95 mg ml<sup>-1</sup>, in THF), hexylamine (36.6 mg ml<sup>-1</sup>, in THF), heptylamine (37 mg ml<sup>-1</sup>, in THF), octylamine (37.23 mg ml<sup>-1</sup>, in THF), decylamine (37.47 mg ml<sup>-1</sup>, in THF), octadecylamine (35 mg ml<sup>-1</sup>, in ethanol) and glucamine (2.5 mg ml<sup>-1</sup>, in DMSO) following our previously reported procedures.<sup>30</sup> After exposing the multilayers to the corresponding amine-containing small molecule solutions for overnight, each modified material was thoroughly washed with ethyl alcohol/THF and exposed to compressed air to dry, prior to further essential characterization or other relevant proof-of-concept demonstrations.

### Physical and chemical durability of the underwater superoleophobicity/superoleophilicity properties

#### Physical durability

1. *Sand drop test.* The 'reactive' multilayer-coated glass slide (1 cm × 1 cm) that was appropriately post-functionalized was immobilized on a large (2 cm × 1.5 cm) glass slide using adhesive tape, where the multilayer coating was exposed to air. The whole system was tilted at 45° prior to pouring a continuous stream of sand grains (100 g) from a height of 20 cm using a funnel. The anti-wetting property of the material was examined by acquiring contact angle measurements and digital images before and after performing the sand drop test.

2. *Sand paper abrasion test.* An abrasive sand paper (grit no. 400; 2 cm × 2 cm) and a post-functionalized multilayer on a glass slide (1 cm × 1 cm) were immobilized on two separate bare microscope glass slides using double sided adhesive tape, where both the abrasive sandpaper surface and the multilayer coating were exposed to air. Next the abrasive sand paper was manually rubbed over the post-functionalized NC multilayer under a 200 g load. Afterwards, the anti-wetting property of the material was examined *via* contact angle measurements and digital imaging using colored DCM.

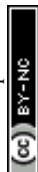
3. *Adhesive tape test.* Double sided adhesive tape (1 cm × 1 cm) was first attached onto a microscope glass slide prior to bringing the adhesive surface into contact with the appropriately post-functionalized multilayer coatings, and a 200 g load was applied on the system to facilitate better, uniform contact of the polymeric coating against the adhesive surface. After 30 min, the polymeric multilayer-coated glass slide was manually peeled off from the adhesive tape surface, and the morphology of the coating and the anti-wetting property of the material were examined by FESEM study and contact angle instruments, respectively.

4. *Effect of freezing on the anti-wetting property.* Deionized water was first degassed under high vacuum in an inert atmosphere (we used argon gas) prior to submerging a multilayer-coated appropriately post-functionalized glass slide (0.6 cm × 0.6 cm). Then, a red colored (due to the added Nile red dye for improved visual inspection) DCM droplet was gently placed on the flat piece of the coated glass slide and kept in a freezer for 2 h at -20 °C. Afterwards, the glass vial was removed from the freezer and the wetting of the model oil droplets was further characterized by acquiring digital images and measuring the contact angles, with the whole frozen system manually tilted at different angles including 0°, 90° and 180°. Furthermore, the whole system was allowed to thaw at room temperature, and the anti-wetting property was examined by measuring the contact angle of the beaded oil droplets.

5. *Effect of heating the aqueous phase on the anti-wetting property.* The multilayer (that consists of 20 bilayers of BPEI/NC) coated glass slide was appropriately post-functionalized prior to being submerged in deionized water (20 ml) in a glass beaker, which was later placed in a water bath (borosil; 450 mm × 150 mm, having 450 ml of tap water). This was again placed on a hot plate, and a mercury thermometer was used for continuous monitoring of the temperature of the system. Next a droplet (8 μl) of red colored DCM was gently placed on the post-functionalized NC multilayer and the temperature of the system was gradually increased up to 100 °C by operating the hot plate. The effect of this gradual heating of the aqueous phase on the anti-wetting property was examined by visual inspections and contact angle measurements.

6. *Effect of water-steam on the anti-wetting property.* The underwater superoleophobic NC multilayer was further exposed to steam for 2 h using a tweezer which was again fixed with a clamp and stand. The steam was generated by boiling tap water (450 ml) at above 100 °C. The effect of this treatment was further investigated by measuring the contact angle of the beaded oil droplets.

**Chemical durability.** The chemical durability of underwater superoleophobicity/superoleophilicity was examined by exposing the glucamine-treated NC multilayers to different harsh and chemically complex conditions including alkaline solution (0.1 M NH<sub>3</sub>; pH 11.13), acidic solution (0.1 M HCl; pH 1), SDS solution (1 mM), DTAB solution (1 mM), BSA solution (5 weight %) and artificial seawater for 10 days. The artificial seawater was prepared by mixing MgCl<sub>2</sub> (0.226 g), MgSO<sub>4</sub> (0.325



g), NaCl (2.673 g) and CaCl<sub>2</sub> (0.112 g) in 100 ml of deionized water in a volumetric flask.

**Coating on various substrates.** Initially, the underwater wetting of oil on various bare substrates (like plastic—made of polyester, wood, sand paper and aluminium foil) was examined to ensure that none of the selected substrates were capable of displaying underwater superoleophobicity/superoleophilicity properties. Next, all the above mentioned substrates were submerged in solutions of BPEI in ethanol overnight, prior to introducing the consecutive LBL deposition of BPEI and NC following the earlier described procedure. The special wetting property in the material was characterized after the appropriate post-chemical modification of the 'reactive' NC multilayers with both glucamine and octadecylamine. Moreover, the interior of a glass tube was also successfully coated with this NC multilayer to achieve the desired underwater superoleophobicity, and this material was further exploited in the demonstration of guided oil droplet transport, which was not possible to achieve with the bare glass tube.

### Cleaning of the oil-contaminated glass substrate

The bare cotton is inherently superoleophobic with an advancing oil contact angle of 169.2° under water. However, ODA-functionalized multilayer-coated cotton was observed to display underwater superoleophilicity with an oil contact angle of 0° under water. This material was further explored in cleaning an oil-contaminated glass substrate under water. First, a bare microscopic glass slide was submerged in a beaker which was filled with deionized water (40 ml), and as expected, upon beading the droplets under water using a syringe, the red-coloured DCM droplets were found to adhere to the bare glass substrate. Then, all the DCM droplets were cleaned/removed instantly from the bare glass substrate by bringing the underwater superoleophilic cotton manually into contact with the DCM droplets that were adhered to the bare glass substrate, whereas uncoated cotton was found to be inappropriate for removing the droplets (see text for more details) as it pushed the droplets from one place to another.

## Acknowledgements

We acknowledge financial support from the Science and Engineering Research Board (YSS/2015/000818). We thank CIF and the Department of Chemistry, Indian Institute of Technology-Guwahati, for their generous assistance in executing various experiments and for the infrastructures. We thank Dr Devasish Chowdhury and the Institute of Advanced Study in Science and Technology (IASST) for their kind help in FESEM characterization of some samples. Miss Dibyangana Parbat thanks the institute for her PhD scholarship. We thank Prof. P. K. Iyer for allowing us to use the Surface Profilometer Instrument.

## References

1 Y. Tian, B. Su and L. Jiang, *Adv. Mater.*, 2014, **26**, 6872.

- 2 Z. Chu, Y. Feng and S. Seeger, *Angew. Chem., Int. Ed.*, 2015, **54**, 2328.
- 3 B. Su, Y. Tian and L. Jiang, *J. Am. Chem. Soc.*, 2016, **138**, 1727.
- 4 M. J. Liu, S. T. Wang, Z. X. Wei, Y. L. Song and L. Jiang, *Adv. Mater.*, 2009, **21**, 665.
- 5 Y. C. Jung and B. Bhushan, *Langmuir*, 2009, **25**, 14165.
- 6 Y. Wu, B. Su, L. Jiang and A. J. Heeger, *Adv. Mater.*, 2013, **25**, 6526.
- 7 Z. Shi, W. Zhang, F. Zhang, X. Liu, D. Wang, J. Jin and L. Jiang, *Adv. Mater.*, 2013, **25**, 2422.
- 8 M. Tao, L. Xue, F. Liu and L. Jiang, *Adv. Mater.*, 2014, **26**, 2943.
- 9 Y. Cai, Q. Lu, X. Guo, S. Wang, J. Qiao and L. Jiang, *Adv. Mater.*, 2015, **27**, 4162.
- 10 K. Chen, S. Zhou and L. Wu, *ACS Nano*, 2016, **10**, 1386.
- 11 A. K. Kota, G. Kwon, W. Choi, J. M. Mabry and A. Tuteja, *Nat. Commun.*, 2012, **3**, 1.
- 12 A. Tuteja, W. Choi, M. L. Ma, J. M. Mabry, S. A. Mazzella, G. C. Rutledge, G. H. McKinley and R. E. Cohen, *Science*, 2007, **318**, 1618.
- 13 H. Bellanger, T. Darmanin, E. T. de Givenchy and F. Guittard, *Chem. Rev.*, 2014, **114**, 2694.
- 14 X. Liu, J. Zhou, Z. Xue, J. Gao, J. Meng, S. Wang and L. Jiang, *Adv. Mater.*, 2012, **24**, 3401.
- 15 Y. Cai, L. Lin, Z. X. Xue, M. J. Liu, S. T. Wang and L. Jiang, *Adv. Funct. Mater.*, 2014, **24**, 809.
- 16 U. Manna and D. M. Lynn, *Adv. Funct. Mater.*, 2015, **25**, 1672.
- 17 L. P. Xu, J. T. Peng, Y. B. Liu, Y. Q. Wen, X. J. Zhang, L. Jiang and S. T. Wang, *ACS Nano*, 2013, **7**, 5077.
- 18 L. Lin, M. J. Liu, L. Chen, P. P. Chen, J. Ma, D. Han and L. Jiang, *Adv. Mater.*, 2010, **22**, 4826.
- 19 Z. Xue, S. Wang, L. Lin, L. Chen, M. Liu, L. Feng and L. Jiang, *Adv. Mater.*, 2011, **23**, 4270.
- 20 S. Gao, J. Sun, P. Liu, F. Zhang, W. Zhang, S. Yuan, J. Li and J. Jin, *Adv. Mater.*, 2016, **28**, 5307.
- 21 F. Zhang, W. B. Zhang, Z. Shi, D. Wang, J. Jin and L. Jiang, *Adv. Mater.*, 2013, **25**, 4192.
- 22 Z. Cheng, H. Lai, Y. Du, K. Fu, R. Hou, C. Li, N. Zhang and K. Sun, *ACS Appl. Mater. Interfaces*, 2014, **6**, 636.
- 23 J. Yong, F. Chen, Q. Yang, U. Farooq and X. Hou, *J. Mater. Chem. A*, 2015, **3**, 10703.
- 24 T. Guo, L. Heng, M. Wang, J. Wang and L. Jiang, *Adv. Mater.*, 2016, **28**, 8505.
- 25 M. Jin, J. Wang, X. Yao, M. Liao, Y. Zhao and L. Jiang, *Adv. Mater.*, 2011, **23**, 2861.
- 26 L. Zhang, Z. Zhang and P. Wang, *NPG Asia Mater.*, 2012, **4**, e8.
- 27 Z. Cheng, H. Lai, Y. Du, K. Fu, R. Hou, C. Li, N. Zhang and K. Sun, *ACS Appl. Mater. Interfaces*, 2014, **6**, 636.
- 28 H. Liu, X. Zhang, S. Wang and L. Jiang, *Small*, 2015, **11**, 3338.
- 29 M. Jin, S. Li, J. Wang, Z. Xue, M. Liao and S. Wang, *Chem. Commun.*, 2012, **48**, 11745.
- 30 E. Zhang, Z. Cheng, T. Lv, Y. Qian and Y. Liu, *J. Mater. Chem. A*, 2015, **3**, 13411.
- 31 R. A. Farrer, C. N. LaFratta, L. Li, J. Praino, M. J. Naughton, B. E. A. Saleh, M. C. Teich and J. T. Fourkas, *J. Am. Chem. Soc.*, 2006, **128**, 1796.



- 32 M. R. Weatherspoon, M. B. Dickerson, G. Wang, Y. Cai, S. Shian, S. C. Jones, S. R. Marder and K. H. Sandhage, *Angew. Chem., Int. Ed.*, 2007, **46**, 5724.
- 33 J. Ford, S. R. Marder and S. Yang, *Chem. Mater.*, 2009, **21**, 476.
- 34 G. Wang, Y. Fang, P. Kim, A. Hayek, M. R. Weatherspoon, J. W. Perry, K. H. Sandhage, S. R. Marder and S. C. Jones, *Adv. Funct. Mater.*, 2009, **19**, 2768.
- 35 S. L. Bechler and D. M. Lynn, *Biomacromolecules*, 2012, **13**, 1523.
- 36 A. M. Rather and U. Manna, *Chem. Mater.*, 2016, **28**, 8689.
- 37 E. Zhang, Z. Cheng, T. Lv, L. Li and Y. Liu, *Nanoscale*, 2015, **7**, 19293.

